

Weierstraß-Institut
für Angewandte Analysis und Stochastik
Leibniz-Institut im Forschungsverbund Berlin e. V.

Preprint

ISSN 2198-5855

**Chirped photonic crystal for spatially filtered optical feedback
to a broad-area laser**

Carsten Brée¹, Darius Gailevičius², Vytautas Purlys², Guillermo Garre Werner^{3,4},
Kestutis Staliunas^{3,5}, Andreas Rathsfeld¹, Gunther Schmidt¹, Mindaugas Radziunas¹

submitted: April 24, 2018

¹ Weierstrass Institute
Mohrenstr. 39
10117 Berlin, Germany
E-Mail: carsten.bree@wias-berlin.de
andreas.rathsfeld@wias-berlin.de
gunther.schmidt@wias-berlin.de
mindaugas.radziunas@wias-berlin.de

² Laser Research Center
Vilnius University
Sauletekio Ave. 10
10222 Vilnius, Lithuania
E-Mail: darius@femtika.lt
vytautas@femtika.lt

³ Departament de Física
Universitat Politècnica de Catalunya
08222 Terrassa, Spain
E-Mail: guillermogarrewerner@gmail.com

⁴ Monocrom S. L.
C/Vilanoveta, 6
08800 Vilanova i la Geltrú, Spain

⁵ Institució Catalana de Recerca i Estudis Avançats
Passeig Lluís Companys 23
08010 Barcelona, Spain
E-Mail: kestutis.staliunas@icrea.cat

No. 2502

Berlin 2018



2010 *Mathematics Subject Classification.* 35B27, 65M80, 78A45, 78A46, 78A60, 78M50.

2010 *Physics and Astronomy Classification Scheme.* 42.60.By, 42.60.Da, 42.60.Fc, 42.60.Jf, 42.70.Qs.

Key words and phrases. External resonators, periodic structure, rigorous coupled wave analysis, inverse scattering problems, semiconductor laser diodes.

This work was supported by the EUROSTARS Project E!10524 HIP-Lasers. This work was supported by “FOKRILAS” (Project No. P-MIP-17-190) from Research Council of Lithuania. We acknowledge fruitful discussions with A. Lamacz, S. Reichelt, B. Schweizer, and H.-J. Wünsche.

Edited by
Weierstraß-Institut für Angewandte Analysis und Stochastik (WIAS)
Leibniz-Institut im Forschungsverbund Berlin e. V.
Mohrenstraße 39
10117 Berlin
Germany

Fax: +49 30 20372-303
E-Mail: preprint@wias-berlin.de
World Wide Web: <http://www.wias-berlin.de/>

Chirped photonic crystal for spatially filtered optical feedback to a broad-area laser

Carsten Brée, Darius Gailevičius, Vytautas Purlys, Guillermo Garre Werner, Kestutis Staliunas, Andreas Rathsfeld, Gunther Schmidt, Mindaugas Radziunas

Abstract

We derive and analyze an efficient model for reinjection of spatially filtered optical feedback from an external resonator to a broad area, edge emitting semiconductor laser diode. Spatial filtering is achieved by a chirped photonic crystal, with variable periodicity along the optical axis and negligible resonant backscattering. The optimal chirp is obtained from a genetic algorithm, which yields solutions that are robust against perturbations. Extensive numerical simulations of the composite system with our optoelectronic solver indicate that spatially filtered reinjection enhances lower-order transversal optical modes in the laser diode and, consequently, improves the spatial beam quality.

Semiconductor laser (SL) diodes with optical feedback from the external cavity (EC) are experimentally and theoretically extensively studied dynamical systems providing a huge variety of different steady and dynamic states [1]. A majority of works on the SL-EC systems are devoted to the study of the transversally-single mode narrow-waveguide SLs, for instance the pioneering work of Lang and Kobayashi [2] has been referred to over 1000 times. In contrast to single lateral (transverse) mode lasers, a substantial width (x -coordinate) of the broad-area (BA) SL diodes leads to supporting multiple lateral optical modes, such that proper modeling of the resulting spatiotemporal dynamics in BASL diodes should be performed by at least 1 (time) + 2 (space) - dimensional partial differential equations [3, 4]. Hence, the detailed experimental and theoretical study of BASL-EC and high-power (HP) BASL-EC devices, in particular, becomes much more complex [4, 5, 6, 7, 8, 9, 10, 11, 12, 13, 14]. Due to potential applications of HP BASLs as high-power optical sources, the majority of works on HP BASL-EC systems are discussing methods for tailoring the emitted beam and improving the beam quality by optical feedback from a properly designed EC [8, 9, 10, 11], study the damages implied by unwanted reinjection of the optical fields [12], or analyze the optical modes governed by the reduced-dimension PDE models [13, 14, 15]. In the present paper, we consider theoretical modelling and numerical studies of a HP-BASL diode subject to optical feedback from a particular type of EC containing an anti-reflection (AR) coated photonic crystal (PhC) as spatial filtering element, see Fig. 1. Our main task here is to efficiently simulate the propagation of the optical field in the EC with an optimized PhC, and to properly calculate the field dynamics in the composite devices of BASL+EC. To simulate the dynamics of BALs we use the 2 (space) + 1 (time) dimensional traveling wave (TW) model [16] and the related parallel solver BALaser [17] developed at the Weierstrass Institute in Berlin and executed on the multicore compute servers there [18]. According to the TW model, the spatiotemporal evolution of the slowly varying complex amplitudes of two waves $E^+(z, x, t)$ and $E^-(z, x, t)$, counterpropagating along the longitudinal axis (z -coordinate), is governed by the following TW equations on the interval $z \in (-l, 0)$,

$$\frac{1}{v_g} \partial_t E^\pm = \left[\mp \partial_z - \frac{i}{2k_0 n} \partial_{xx} - i\beta \right] E^\pm + F_{sp}^\pm, \quad (1a)$$

$$E^+(-l, x, t) = \sqrt{R_r} E^-(-l, x, t), \quad (1b)$$

$$E^-(0, x, t) = \sqrt{R_f} E^+(0, x, t) + (1 - R_f) [\mathcal{F} E^+](x, t). \quad (1c)$$

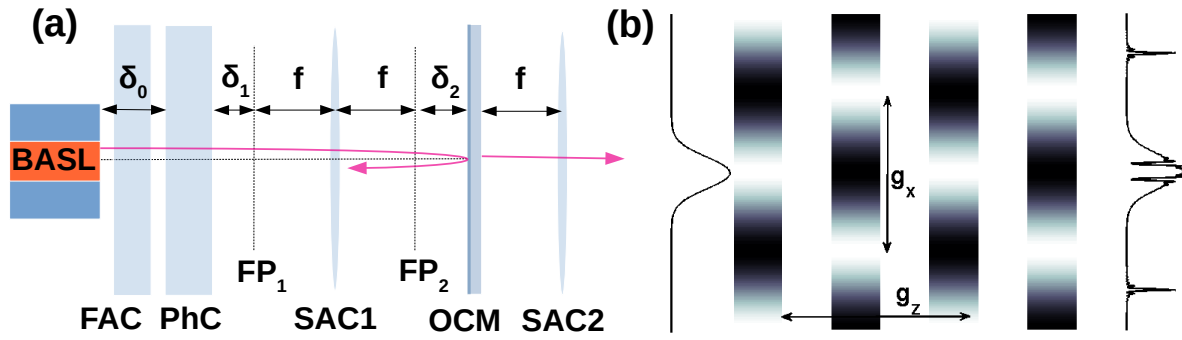


Figure 1: (a) Sketch of considered BASL-EC setup: diode laser, fast axis collimator (FAC), PhC, slow axis collimating lenses (SAC), output coupler mirror (OCM). Dashed: front and rear SAC1 focal planes, with offsets δ_1 , δ_2 from PhC and OCM, respectively. δ_0 : distance between BASL and PhC. (b): scheme of PhC, incident (left) and transmitted beams (right) in k_x -space.

Here, v_g , $k_0 = 2\pi/\lambda_0$, \bar{n} , and F_{sp}^\pm are the group velocity of light, the free-space central wavenumber for an employed wavelength $\lambda_0 = 975$ nm, the reference refractive index, and the Langevin noise term, respectively. The complex propagation factor $\beta(z, x, t)$ accounts for linear and nonlinear (two-photon) absorption [19], the initially induced refractive index profile, and the refractive index in the semiconductor material. The last two factors depend on the excess carrier density and take into account nonlinear gain compression [19], material gain dispersion [20], and the static refractive index change due to Joule heating [3]. The dynamics of the carrier densities is governed by the diffusive rate equation where carrier diffusion and injected current (pump) at the active zone are determined by solving the carrier spreading problem in the lateral (x) and vertical (y) cross-sections of the BASL device simultaneously [21]. Parameters R_r and R_f (which are 0.95 and 0.04 in the example considered below) are the field intensity reflection and transmission at the rear and front facets $z = -l$ and $z = 0$ of the diode (l : the length of the BASL), *cf.* Refs. [19, 16] for more details on the model and typical diode parameters.

Assuming that the index guiding along the vertical axis of the BASL as well as the beam collimation by the FAC are perfect, the optical feedback \mathcal{F} in Eq. (1c) is given in terms of a general linear integral operator,

$$[\mathcal{F}E^+](x, t) = \int_{-\infty}^t \int_{\mathbb{R}} K(x', t', x, t) E^+(0, x', t') dx' dt', \quad (2)$$

where the kernel function $K(x', t', x, t)$ depends on the configuration of the EC. For its construction, we exploit Huygens-Fresnel integrals within each optical element, see Fig. 1(a). For a perfect EC with vanishing offsets and no PhC [22], this procedure implies $K(x', t', x, t) = \eta \delta(x + x') \delta(t' - t + \tau)$, where δ is the Dirac delta function, τ is the field roundtrip time in the EC, and η accounts for the field reflectivity at the OCM and the constant phase shifts at the SAC lens.

For extensive numerical calculation of the compound system, it is crucial to derive efficient approximations of the kernel function K in (2). To model the PhC part of the optical propagation within the EC, we investigate two different models for optical transmission through and backscattering from the PhC. The first, and more complex, of these models relies on the solution of Maxwell's equations. The corresponding linear kernel K_{PhC} which enters the overall kernel K , is, in general, nonlocal in time and space. Our second model is determined by a beam propagation method (BPM), which neglects backscattering as well as angular dependencies of optical pathlengths. The resulting kernel K is local in time, which is beneficial for its implementation into our solver. A comparison of these two models reveals conditions under which the BPM provides a reasonable approximation. A previously reported

good agreement of measurements and BPM-based simulations of the single pass transmission of the optical field through the optimized PhC [23] allows us to trust in the BPM. Since suitably manufactured PhCs bear a strong potential for tailoring the far-field characteristics of a transmitted beam [24], we focus on modelling and efficient implementation of the kernel function K and the resulting delay term (2) into our parallel solver [17].

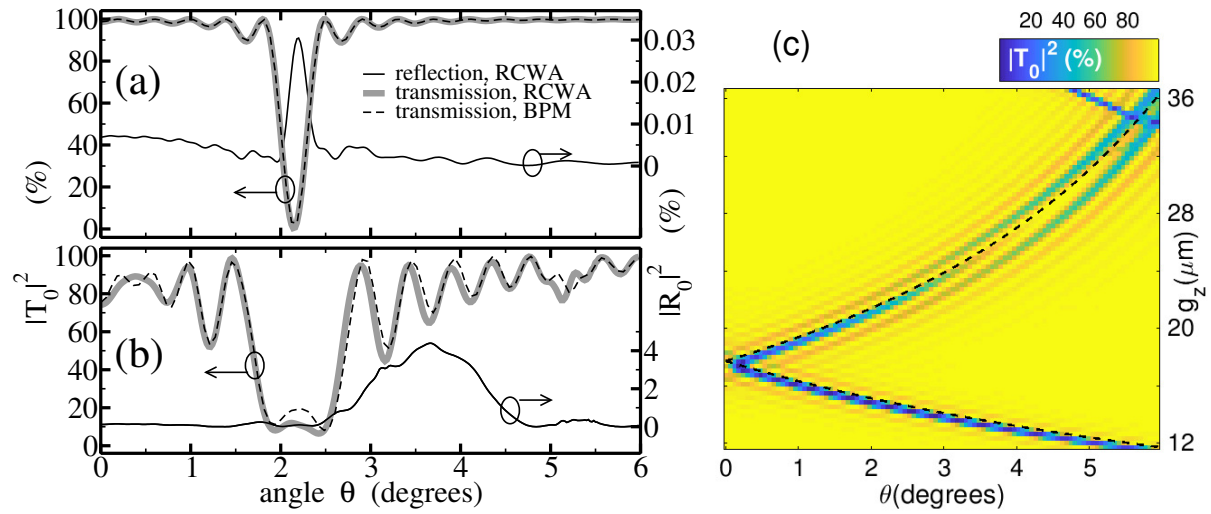


Figure 2: Parameter study for PhC with $g_x = 2.4\mu\text{m}$ and 24 periods along z . (a): $|T_0|^2$ (thick gray) and $|R_0|^2$ (thin black), RCWA. Dashed: $|T_0|^2$, BPM. PhC parameters: $\Delta n_0 = 0.004$, $g_z = 21.4\mu\text{m}$ (b): same, but $\Delta n_0 = 0.02$. (c): $|T_0|^2$ versus θ and g_z , $\Delta n_0 = 0.006$. Dashed: filtering angles vs. g_z , Eq. (3).

For an accurate description of light propagation through a periodically modulated medium, one has to solve a boundary value problem for the time-harmonic Maxwell system and an incident plane wave of prescribed polarization, incident angle, and wavelength. While a rigorous mathematical solution of the corresponding Sommerfeld radiation problem has only recently been achieved for the case of a PhC in a semi-infinite half-space [25], numerical approaches for calculating complex reflection and transmission amplitudes R_j, T_j for each diffraction order j are well established. Here, we employ the method of rigorous coupled-wave analysis (RCWA). The time-harmonic Maxwell system is rewritten as an ordinary differential equation for the vector of z -dependent lateral Fourier coefficients of the transversal electro-magnetic field components. The underlying domain is split into several slices s.t. the refractive index is z -independent in each slice, and, for each slice, the differential equation can be solved by an eigenvalue decomposition. For PhCs with low contrast and smooth variation of \bar{n} in the transversal x -direction, as considered in this work, *cf.* Fig. 1(b), the Fourier-mode expansion of the field can be truncated to a small number of modes without losing much accuracy, *cf.* [26, 27, 28]. For the simulation, we choose a PhC with background refractive index $\bar{n} = 1.5$ and lateral period $g_x = 2.4\mu\text{m}$. To confirm the effect of spatial filtering by resonant scattering into higher diffraction orders, we performed calculations for different values of index modulation depth Δn_0 . In Fig. 2(a), we show the obtained transmission efficiency $|T_0|^2$, for a PhC with index modulation $\Delta n_0 = 0.004$ and 24 longitudinal periods with $g_z = 21.4\mu\text{m}$. In case of small incidence angles θ , resonant deflection of optical energy from the central lobe to the first diffraction orders occurs at

$$\sin \theta = \pm \frac{\lambda_0}{2g_x} |Q - 1|, \quad (3)$$

with a geometric resonance factor $Q = 2g_x^2 \bar{n} / g_z \lambda_0$, *cf.* [29]. For the chosen PhC parameters, this resonance condition results in filtering angles at 2° . The AR coatings suppress reflections from the

PhC-air interfaces, which reveals only weak resonant backscattering $< 0.04\%$ from within the PhC, see thin black curve in Fig. 2(a). For increased index modulation of $\Delta n_0 = 0.02$, the transmission efficiency $|T_0|^2$ is shown in panel (b), with a considerably broader transmission gap around 2° . The corresponding backscattering efficiency $|R_0|^2$ shows a massive increase to about 4% , comparable to the reflectivity of the OCM. For suppressing divergent lateral modes with spatially filtered feedback, such a large amount of backscattering is unacceptable.

Finally, we calculated $|T_0|^2$ versus longitudinal period g_z in an angular range $|\theta| < 6^\circ$, the typical beam divergence of semiconductor laser diodes, *cf.* Fig. 2(c). Again, we observe sharp transmission gaps at angles depending on g_z . In fact, closer inspection of Eq. (3) yields two branches for the filtering angle as a function of g_z . These are shown as dashed lines for fixed wavelength λ_0 , $g_x = 2.4\mu\text{m}$, and $\bar{n} = 1.5$. A comparison with RCWA results shows that Eq. (3) accurately predicts the angular positions of the transmission gaps.

While the RCWA provides an accurate solution of the time-harmonic Maxwell equations, the computationally fast, but approximate BPM is more suitable for the subsequent optimization calculations. In paraxial approximation, it can be derived from the TW equation (1a) for the forward field component E^+ , upon eliminating all nonlinear and dispersive contributions to the propagation constant and polarization density. Instead, only the contribution of refractive index modulation $\Delta n(x, z)$ is taken into account. As the PhC excites radiation at large lateral angles, we increase the accuracy of our BPM by replacing the paraxial diffraction operator $\sim \partial_{xx}$ in Eq. (1a) by a pseudo-differential operator[30], which accurately accounts for the forward-branch $k_0 > 0$ of the spatial dispersion relation $k_x^2 + k_z^2 = k_0^2$. The resulting PDE, which is first-order w.r.t. z , is an envelope approximation of the second-order Helmholtz equation. For given initial condition $\hat{E}(k_x, z_0)$, the initial value problem has the general solution $\hat{E}(k_x, z) = \sum_{j=-J}^J T_j(k_x; z, z_0) \hat{E}(k_x + 2\pi j/g_x, z_0)$, with complex transmission amplitudes T_j for the j -th diffraction order. The introduced truncation threshold J accounts for the fact that the intensity scattered into higher-order sidebands ($J \gtrsim 2$) is negligible for the considered weak contrast PhCs. Therefore, the PhC propagator \hat{K}_{PhC} has a sparse, $(2J + 1)$ -banded matrix structure, where here and in the following, the caret denotes k_x -space counterparts of linear integral operators. The complex amplitudes T_j can be obtained by semi-analytic integration of the envelope equation for suitable initial conditions, using an eigenvector decomposition technique[31]. With the obtained PhC propagator \hat{K}_{PhC} , we can proceed to build a matrix model for the overall EC kernel K , Eq. (2). First of all, the RCWA results indicate a negligible wavelength dependence of transmission and reflection efficiencies of the considered AR-coated PhCs in a spectral interval around $\lambda_0 = 975\text{ nm}$, with a length $\Delta\lambda \approx 5\text{ nm}$ identical to the characteristic spectral bandwidth of the BASL emission, with the noted exception of PhCs exhibiting pronounced resonant backscattering. Since the latter are of little practical use for the current study, it is admissible to assume that the full kernel is local in time,

$$K(x', t', x, t) = \bar{K}(x', x) \delta(t' - t + \tau) \quad \Rightarrow \quad [\mathcal{F}E^+](x, t) = \int_{\mathbb{R}} \bar{K}(x', x) E^+(0, x', t - \tau) dx'.$$

On the discrete numerical level, the last integral expression is equivalent to the matrix-vector product,

$$[\mathcal{F}E^+]_h(t) = \bar{\mathbf{K}}_h E_h^+(0, t - \tau),$$

where the subscript index h stands for discrete space in the lateral x -direction, the vector-functions $E_h^+(0, t - \tau)$ and $[\mathcal{F}E^+]_h(t)$ represent the (discretized) emitted and the reinjected fields at the front facet of the diode, whereas $\bar{\mathbf{K}}_h$ is a large $(N_x \times N_x)$ -dimensional matrix (N_x : number of equidistant lateral discretization steps in the considered computational domain). The matrix $\bar{\mathbf{K}}_h$ can be further factorized as $\bar{\mathbf{K}}_h = \mathbf{K}_b \mathbf{K}_c \mathbf{K}_f$. Here, $\mathbf{K}_f, \mathbf{K}_b$ are forward resp. backward propagators given by

$$\mathbf{K}_f = \mathbf{K}_{\delta_1} \mathbf{K}_{\text{PhC}} \mathbf{K}_{\delta_0}, \quad \mathbf{K}_b = \mathbf{K}_{\delta_0} \mathbf{K}_{\text{PhC}} \mathbf{K}_{\delta_1}.$$

with discrete, x -space counterpart \mathbf{K}_{PhC} of the PhC propagator \hat{K}_{PhC} introduced above, and $\mathbf{K}_{\delta_0}, \mathbf{K}_{\delta_1}$ propagate through the laterally homogeneous media (FAC, air gaps), *cf.* Fig. 1 (a). In k_x -space, $\hat{\mathbf{K}}_f, \hat{\mathbf{K}}_b$ have a sparse, band matrix structure inherited from $\hat{\mathbf{K}}_{\text{PhC}}$, which is beneficial for numerical evaluation. The propagator \mathbf{K}_c propagates from focal plane FP1 towards the OCM and back. In x -space, it is anti-diagonal and yields a mirror image of the complex optical field, multiplied, for non-vanishing offset δ_2 , by a phase factor with parabolic dependence on x *cf.* [15]. For compactness of presentation, we introduce a matrix representation \mathbf{D} of the discrete Fourier transform (DFT) which maps from x to k_x -space. With this, our numerical algorithm for computation of the optical reinjection is given by

$$[\mathcal{F}E_h^+](0, t) = [\mathbf{D}^{-1}\hat{\mathbf{K}}_b\mathbf{D}\mathbf{K}_c\mathbf{D}^{-1}\hat{\mathbf{K}}_f\mathbf{D}]\mathbf{E}^+(0, t - \tau), \quad (4)$$

For simulating the optical field and carrier dynamics in the BASL subject to filtered reinjection, the factors $\mathbf{K}_c, \hat{\mathbf{K}}_b, \hat{\mathbf{K}}_f$ are initially precalculated and fed into our optoelectronic solver. With respect to numerical complexity of our modeling approach, we emphasize that the action of the DFT matrix \mathbf{D} is calculated using the Cooley and Tukey fast Fourier transform (FFT) algorithm. In consequence, instead of $\sim N_x^2$ operations required for matrix-vector multiplication, the described factorization of $\hat{\mathbf{K}}_h$ significantly reduces the numerical complexity ($\sim N_x \ln N_x$).

It remains to identify the limits of validity of the BPM used for modeling the PhC propagators contained in K . For each of the PhC structures in Fig. 2, we calculate the corresponding transmission efficiencies. As shown by the black curve in Fig. 2(a), we observe excellent agreement for low index contrast $\Delta n_0 = 0.004$, and slightly larger deviations for $\Delta n_0 = 0.02$, *cf.* Fig. 2(b), which is prohibitive due to large resonant backscattering. Altogether, extensive simulations with the RCWA solver reveal that the BPM yields reasonable results for lateral periods $g_x \gtrsim 2\mu\text{m}$ (i.e., larger than approximately twice the wavelength), longitudinal periods g_z corresponding to $Q \in [0.4, 1.6]$, refractive index contrast of the order of $\Delta n \sim 0.01$, and not more than some ten longitudinal periods. In that case, the RCWA also predicts a tolerable intensity in the backscattered field below the 1%-level.

The above considerations indicate that broader angular transmission gaps, which are potentially useful for spatial filtering, are obtained either for larger index contrast or increased number of longitudinal layers. However, in case of strictly periodic PhCs, this comes at the cost of increased resonant backscattering. In the following, we show that PhCs with variable longitudinal periods avoid this detrimental side effect. The use and versatility of longitudinally chirped PhCs for spatial filtering of laser beams has first been discussed in [31, 32]. Here, we solve the inverse problem of finding an optimized longitudinal chirp for a prescribed transmission efficiency $|T_0|^2$ with broad angular gaps. Using a suitable nonlinear optimization routine, we maximize a fitness functional $F : \vec{d}_z \in \mathbb{R}^N \rightarrow \mathbb{R}^+$, *cf.* [30]. Here, the N components d_z^j of \vec{d}_z correspond to longitudinal layer thicknesses, where each layer consists of two slices of thickness $d_z^j/2$, namely, a slice with harmonic lateral index modulation $\bar{n} + \Delta n$ and a homogeneous slice with refractive index \bar{n} . Between adjacent layers, there is a π -phaseshift in the modulated slice. The fitness functional favors vectors \vec{d}_z leading to chirped PhCs with admissible transmission efficiency $|T_0|^2$ smaller than 20% between 2° and 4° , but unity transmission outside of this interval. The total angular range in consideration is $[0^\circ, 6^\circ]$. For the current study, we used a fixed refractive index modulation depth of $\Delta n_0 = 0.012$ and $N = 48$ longitudinal layers. For optimization, we use a genetic algorithm, which is known to prevent convergence to a narrow local minimum and favors robust solutions [33]. Each iteration step of the genetic algorithm requires calculations of $|T_0|^2$ and $F[\vec{d}_z]$ for all members \vec{d}_z of the genetic pool. For this, we employ the numerically more efficient BPM and compare the final optimization result with the RCWA. In Fig. 3, we present an optimization result obtained for an admissible transmission of 20%. The optimized chirp vector \vec{d}_z^{opt} is shown in panel (a), and the resulting transmission efficiency is depicted by the dashed curve in panel (b), with broad transmission gap between 2° and 4° . The thick gray line in panel (b) corresponds to the

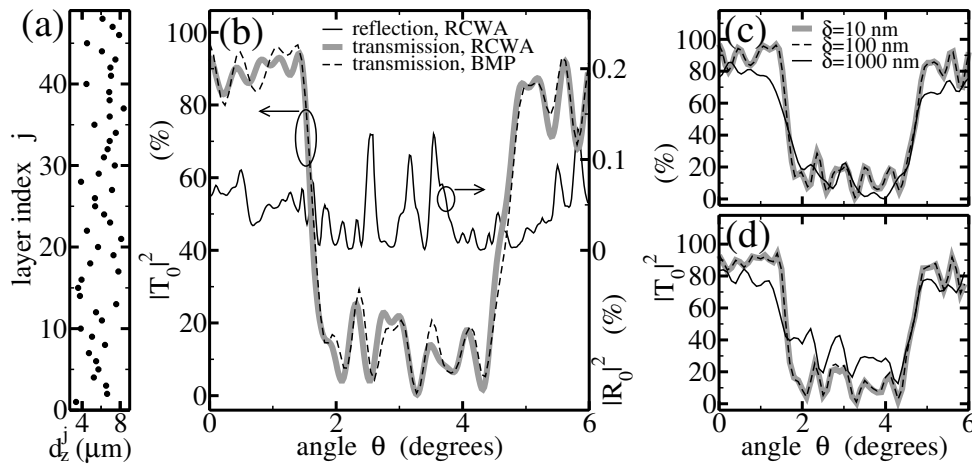


Figure 3: (a): optimized chirp $\vec{d}_z^{\text{opt.}}$. (b): corresponding transmission efficiency $|T_0|^2$. Thick gray: RCWA, thin black: BPM, dotted line: $|R_0|^2$. (c): $|T_0|^2$ for perturbed chirp $\vec{d}_z^{\text{opt.}} + \vec{\xi}_\delta$ (BPM), $\delta = 10$, 100, and 1000 nm (gray, dashed, solid black). (d): same as (c), RCWA

transmission amplitude obtained by feeding $\vec{d}_z^{\text{opt.}}$ into the RCWA solver. It exhibits reasonable agreement with BPM results. Furthermore, the corresponding reflection efficiency does not exceed 0.13% in the considered angular range, *cf.* panel (b). Finally, robustness of the optimized solution versus perturbations is established numerically. Forty displacement vectors $\vec{\xi}_\delta \in \mathbb{R}^N$ are drawn randomly, with components uniformly distributed in $[-\delta, \delta]$, and added to $\vec{d}_z^{\text{opt.}}$. Transmission efficiencies, averaged over the realizations of $\vec{\xi}_\delta$, are depicted in panels (d) (BPM) and (e) (RCWA), for $\delta = 10$ nm, $\delta = 100$ nm and $\delta = 1000$ nm. We find remarkable robustness, with a noise tolerance well within the current accuracy limits of direct femtosecond laser writing[30].

Finally, we simulated an example of a 1 mm-long and 100 μm -broad HP BASL diode with and without the feedback from the EC containing the optimized PhC filter, see Fig. 4. The bias current of this laser was 2.8 A. In absence of the EC, it emits a high-power $P_0 = 2.82$ W beam with divergence angle $\theta_{95} \sim 6^\circ$ and near field with $w_{95} = 92 \mu\text{m}$, both evaluated at 95% power content. The lateral beam parameter product (BPP) and beam quality factor amount to $\text{BPP}_0 \sim 2.25 \text{ mm} \times \text{mrad}$ and $M_0^2 = \text{BPP}_0 \times \pi/\lambda \sim 7.3$, respectively. The brightness is $B_0 = P_0^2/M_0^2\lambda^2 \approx 0.4 \text{ W/sr} \cdot \mu\text{m}^2$, where it was assumed that the beam is diffraction limited in the vertical direction.

Next, we have simulated BASL with the EC containing the optimized PhC. Substituting the PhC with a homogeneous glass block of the same dimensions and background refractive index, 1 : 1 imaging of the mirrored field configuration would be obtained for vanishing EC offsets δ_2 and $\Delta_1 := \delta_0 - l_{\text{FAC}}(1 - 1/\bar{n}_{\text{FAC}}) + l_{\text{PhC}}/\bar{n}_{\text{PhC}} + \delta_1 = 0$ for a perfectly aligned EC. The total width and the background refractive index of the considered PhC and FAC were $l_{\text{PhC}} = 0.289$ mm, $\bar{n}_{\text{PhC}} = 1.5$, and $l_{\text{FAC}} = 1.5$ mm, $\bar{n}_{\text{FAC}} = 1.5$, respectively, whereas the focal length of the SAC lenses was $f = 24$ mm. We performed simulations for $\delta_2 = 0$ and different values of the offset Δ_1 . Optimal beam quality w.r.t. beam parameter product and beam brightness was achieved for $\Delta_1 \approx 1.5$ mm, *cf.* Fig. 4(a). Due to the radiation loss to the sidebands, see insert, a significant power fraction is lost from the central lobe, i.e., it contains only 78% of the total emitted power $P_{\text{tot.}} = 2.6$ W. Nevertheless, as a main achievement of our theoretical study, we find that the spatially filtered optical feedback causes a significant improvement of the laser beam quality. In Fig. 4(b), we show the relative changes of brightness and beam quality factor M^2 compared to the corresponding factors B_0 and M_0^2 without reinjection. At optimum, the simulations show that brightness increases by 45%, while M^2 decreases by 50%. It is noteworthy that a significant shaping of the angular beam profile can be observed not

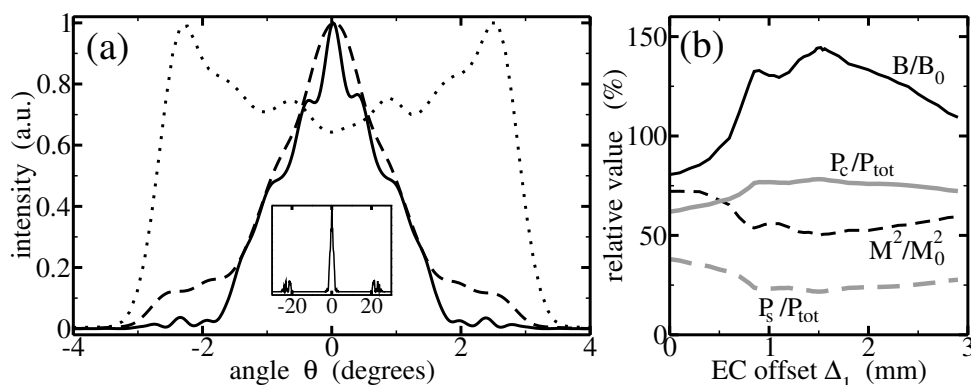


Figure 4: (a): BASL emission for $\Delta_1 = 1.5$ mm. Dashed: time-averaged Fourier transformed near field at BASL output facet. Solid: far field coupled out from EC. Dotted: BASL emission w/o EC. Insert: same, on larger angular scale. (b) brightness B (black solid), M^2 (black dashed) relative to case w/o EC. Gray, solid resp. dashed: power fractions P_c/P_{tot} , P_s/P_{tot} in central- and sidelobes.

only after its pass through the PhC but also directly after its emission from the diode, see dashed and solid black curves in Fig. 4(a). This observation confirms the suppression of the higher-order lateral optical modes of the HP BASL diode by an adequately designed spatially filtered optical feedback.

In conclusion, we have considered the BASL-EC system operating at the high-power regime. We have performed efficient modeling and optimization of the beam propagation in the EC containing a PhC spatial filtering element. We have shown that provided the refractive index contrast in the PhC is not exceeding the order of 10^{-2} , the backscattered intensity can be kept below 1% and the BPM can produce reliable field transmissions through the PhC. Our optimization of the PhC was aiming to reduce the radiation at $\pm[2^\circ, 4^\circ]$ angles to the optical axis during the single-pass of the beam through the PhC. The consequent simulations of the HP BASL-EC system with this optimized PhC within the EC have demonstrated the suppression of the higher-order lateral optical modes of the HP BASL diode. A more detailed study of the impact of filtered feedback to the beam quality of HP BASL diodes will be considered elsewhere.

References

- [1] D.M. Kane and A. Shore, editors. *Unlocking Dynamical Diversity: Optical Feedback Effects on Semiconductor Lasers*. John Wiley & Sons, 2005.
- [2] R. Lang and K. Kobayashi. External optical feedback effects on semiconductor injection laser properties. *IEEE J. of Quantum Electron.*, 16:347–355, 1980.
- [3] H. Wenzel. Basic aspects of high-power semiconductor laser simulation. *IEEE J. Sel. Top. Quantum Electron.*, 19(5):1–13, 2013.
- [4] C. Simmendinger, D. Preier, and O. Hess. Stabilization of chaotic spatiotemporal filamentation in large broad area lasers by spatially structured optical feedback. *Opt. Express*, 5:48–54, 1999.
- [5] J.J. Lim, S. Sujecki, L. Lang, Z. Zhang, D. Paboeuf, G. Pauliat, G. Lucas-Leclin, P. Georges, R.C.I. MacKenzie, P. Bream, S. Bull, K.-H. Hasler, B. Sumpf, H. Wenzel, G. Erbert, B. Thestrup, P.M. Petersen, N. Michel, M. Krakowski, and E.C. Larkins. Design and simulation of next-generation

- high-power, high-brightness laser diodes. *IEEE J. Sel. Top. Quantum Electron.*, 15:993–1008, 2009.
- [6] S.K. Mandre, I. Fischer, and W. Elsässer. Spatiotemporal emission dynamics of a broad-area semiconductor laser in an external cavity: stabilization and feedback-induced instabilities. *Optics Communications*, 244:355–365, 2005.
- [7] S. Wolff, A. Rodionov, V.E. Sherstobitov, and H. Fouckhardt. Fourier-optical transverse mode selection in external-cavity broad-area lasers: experimental and numerical results. *IEEE J. Quantum Electron.*, pages 448–458, 2003.
- [8] N. Gaciu, E. Gehrig, and O. Hess. Control of broad-area laser dynamics with delayed optical feedback. In E. Schöll and H. G. Schuster, editors, *Handbook of Chaos Control*, pages 427–453. Wiley VCH Verlag GmbH & Co. KGaA, 2008.
- [9] A. Jechow, M. Lichtner, R. Menzel, M. Radziunas, D. Skoczowsky, and A. Vladimirov. Stripe-array diode-laser in an off-axis external cavity: Theory and experiment. *Optics Express*, 17(22): 19599–19604, 2009.
- [10] C. Zink, M. Niebuhr, A. Jechow, A. Heuer, and R. Menzel. Broad area diode laser with on-chip transverse bragg grating stabilized in an off-axis external cavity. *Optics Express*, 22: 14108–14113, 2014.
- [11] H. Fouckhardt, A.-K. Kleinschmidt, J. Strassner, and C. Doering. Fundamental transverse mode selection (tms#0) of broad area semiconductor lasers with integrated twice-retracted 4f set-up and film-waveguide lens. *Advances in OptoElectronics*, 2017:5283850, 2017.
- [12] M. Hempel, M. Chi, P.M. Petersen, U. Zeimer, and J.W. Tomm. How does external feedback cause algaas-based diode lasers to degrade? *Appl. Phys. Lett.*, 102:023502, 2013.
- [13] J.R. Marciante and G.P. Agrawal. Lateral spatial effects of feedback in gain-guided and broad-area semiconductor lasers. *IEEE J. Quantum Electron.*, 32:1630–1635, 1996.
- [14] A. Takeda, R. Shogenji, and J. Ohtsubo. Spatial-mode analysis in broad-area semiconductor lasers subjected to optical feedback. *Optical Review*, 20(4):308–313, 2013.
- [15] Y. Champagne, S. Mailhot, and N. McCarthy. Numerical procedure for the lateral-mode analysis of broad-area semiconductor lasers with external cavity. *IEEE J. Quantum Electron.*, 31:795–810, 1995.
- [16] M. Spreemann, M. Lichtner, M. Radziunas, U. Bandelow, and H. Wenzel. Measurement and simulation of distributed-feedback tapered master-oscillator power amplifiers. *IEEE J. of Quantum Electron.*, 45:609–616, 2009.
- [17] see <http://www.wias-berlin.de/software/BALaser> for more information about our optoelectronic solver; accessed April 11, 2018.
- [18] M. Radziunas. Modeling and simulations of broad-area edge-emitting semiconductor devices. *The Int. J. of High Perform. Comp. Appl.*, First online December 23, 2016. doi: 10.1177/1094342016677086. URL <https://doi.org/10.1177/1094342016677086>.

- [19] A. Zeghuzi, M. Radziunas, A. Klehr, H.-J. Wünsche, H. Wenzel, and A. Knigge. Influence of non-linear effects on the characteristics of pulsed high-power broad-area distributed bragg reflector lasers. *Opt. and Quantum Electron.*, 50:88, 2018.
- [20] U. Bandelow, M. Radziunas, J. Sieber, and M. Wolfrum. Impact of gain dispersion on the spatio-temporal dynamics of multisection lasers. *IEEE J. of Quantum Electron.*, 37:183–188, 2001.
- [21] M. Radziunas, A. Zeghuzi, J. Fuhrmann, Th. Koprucki, H.-J. Wünsche, H. Wenzel, and U. Bandelow. Efficient coupling of the inhomogeneous current spreading model to the dynamic electro-optical solver for broad-area edge-emitting semiconductor devices. *Optical and Quantum Electronics*, 49:332, 2017.
- [22] S. Wolff, D. Messerschmidt, and H. Fouckhardt. Fourier-optical selection of higher order transverse modes in broad area lasers. *Opt. Express*, 5:32–37, 1999.
- [23] D. Gailevicius, V. Koliadenko, V. Purlys, M. Peckus, V. Taranenko, and K. Staliunas. Photonic crystal microchip laser. *Sci. Rep.*, 6:34173, 2016. doi: 10.1038/srep34173.
- [24] Lina Maigyte and Kestutis Staliunas. Spatial filtering with photonic crystals. *Appl. Phys. Rev.*, 2(1):011102, 2015. doi: 10.1063/1.4907345.
- [25] A. Lamacz and B. Schweizer. Outgoing wave conditions in photonic crystals and transmission properties at interfaces. *arXiv:1509.00683v2 [math.AP]*, 2016.
- [26] E. Popov. Chapter 7: Differential theory of periodic structures. In E. Popov, editor, *Gratings: Theory and Numerical Applications*, chapter 7. Presses Universitaires de Provence, Aix Marseille Université, Institut Fresnel UMR 7249, 2014.
- [27] M. G. Moharam and T. K. Gaylord. Rigorous coupled wave analysis of planar-grating diffraction. *J. Opt. Soc. Amer.*, 71:811–818, 1981.
- [28] M. Nevière and E. Popov. *Light propagation in periodic media*. Marcel Dekker, Inc., New York, Basel, 2003.
- [29] M. Radziunas, R. Herrero, M. Botey, and K. Staliunas. Far field narrowing in spatially modulated broad area edge-emitting semiconductor amplifiers. *J. Opt. Soc. Am. B*, 32(5):993–1000, 2015.
- [30] Darius Gailevičius, Vytautas Purlys, Martynas Peckus, Roaldas Gadonas, and Kestutis Staliunas. Spatial filters on demand based on aperiodic photonic crystals. *Annalen der Physik*, 529(8):1700165–n/a, 2017. ISSN 1521-3889. doi: 10.1002/andp.201700165. URL <http://dx.doi.org/10.1002/andp.201700165>. 1700165.
- [31] Kestutis Staliunas and Victor J. Sánchez-Morcillo. Spatial filtering of light by chirped photonic crystals. *Phys. Rev. A*, 79(5):053807, 2009. doi: 10.1103/physreva.79.053807.
- [32] V. Purlys, L. Maigyte, D. Gailevičius, M. Peckus, M. Malinauskas, and K. Staliunas. Spatial filtering by chirped photonic crystals. *Phys. Rev. A*, 87(3):033805, 2013. doi: 10.1103/physreva.87.033805.
- [33] David B. Fogel. *Evolutionary Computation: Toward a New Philosophy of Machine Intelligence*. Wiley-IEEE Press, New York, Basel, 3rd edition edition, 2006.